Short Papers

Dispersion Characteristics of Grooved Microstrip Line (GMSL)

W. Chamma, N. Gupta, and L. Shafai

***Abstract*—In this paper, the method of lines and finite-difference time-domain numerical methods are used to investigate the field distribution, dispersion, and impedance characteristics of the grooved microstrip line (GMSL) structure. It is found that the GMSL is less dispersive compared to conventional microstrip lines, and also provides a wide range of characteristic impedance values as a function of the groove width. Increasing the groove width of the microstrip structure can also reduce the dielectric and conductor losses of the GMSL.**

***Index Terms*—FDTD method, method of lines, microstrip line, numerical methods.**

I. Introduction

Microstrip lines are widely used in microwave circuits and antennas feed systems. Among various microstrip configurations, the suspended microstrip lines [1], [2] have always been a topic of interest for researchers because of low-loss configuration and for being less dispersive. These important features make it eminently suitable for use at millimeter-wave frequencies.

Generally, practical suspended lines employ grooves in the sidewalls of the metallic enclosure to support the dielectric substrate. A grooved line [3]–[5] basically extends the idea of suspended microstrip lines and provides a better solution for construction and assembly of these types of lines. Thus, instead of providing grooves in the sidewalls of the enclosure, the printed substrate is mounted over the grooved dielectric substrate. For larger groove dimensions, the dispersion and impedance characteristics of the grooved line remains close to the conventional suspended-line case.

The concept of grooved structure is not new in monolithic-microwave integrated-circuit (MMIC) technology and is implemented using micromachining technology [6], [7]. In [8], a new type of monolithic planar transmission line, i.e., microshield line, has been proposed. The removal of the silicon substrate material in the vicinity of the metal structures significantly improves the insertion-loss characteristics, frequency-response bandwidth, transmission-line dispersion characteristics, and impedance control capability. Similar improvement is found to be true for the microwave integrated circuits (MIC's) well. The performance characteristics of such lines, such as dispersion and impedance characteristics, mainly depend on the groove dimensions. Therefore, to achieve an optimum performance of this line, it is necessary to investigate its various characteristics for different groove dimensions.

In this paper, two numerical techniques, i.e., the method of lines (MOL) and the finite-difference time-domain (FDTD), have been utilized to study the grooved-line structure in an enclosed, as well as open-space environment, respectively. The grooves have been considered to be uniform along the line, i.e., the direction of propagation, having a depth up to the bottom ground plane. At first, a detailed field distribution is presented using the FDTD. The dispersion and

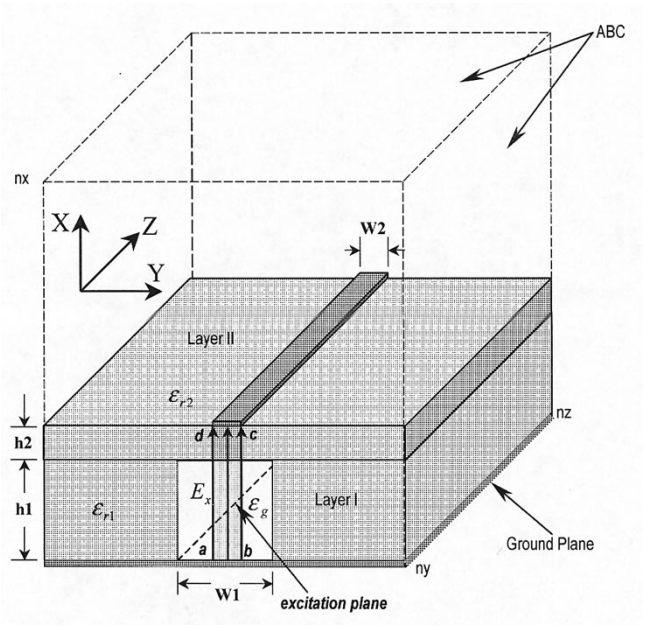

Fig. 1. Geometry of the GMSL structure inside a FDTD lattice.

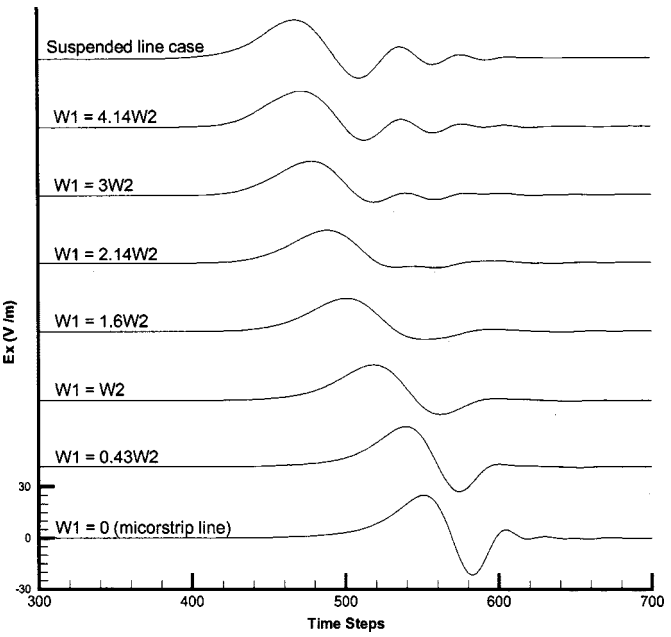

Fig. 2. E_x-field component below the strip line of GMSL for different groove widths at $k = 150dz$.

Manuscript received June 22, 1998.

W. Chamma is with the Microwave Analysis and Countermeasures Group, Defence Research Establishment Ottawa (DREO), Ottawa, Ont., Canada K1A 0Z4.

N. Gupta is with the Department of Electronics and Communication Engineering, Birla Institute of Technology, Ranchi, India.

L. Shafai is with the Department of Electrical and Computer Engineering, University of Manitoba, Winnipeg, Man., Canada R3T 5V6.

Publisher Item Identifier S 0018-9480(00)02778-2.

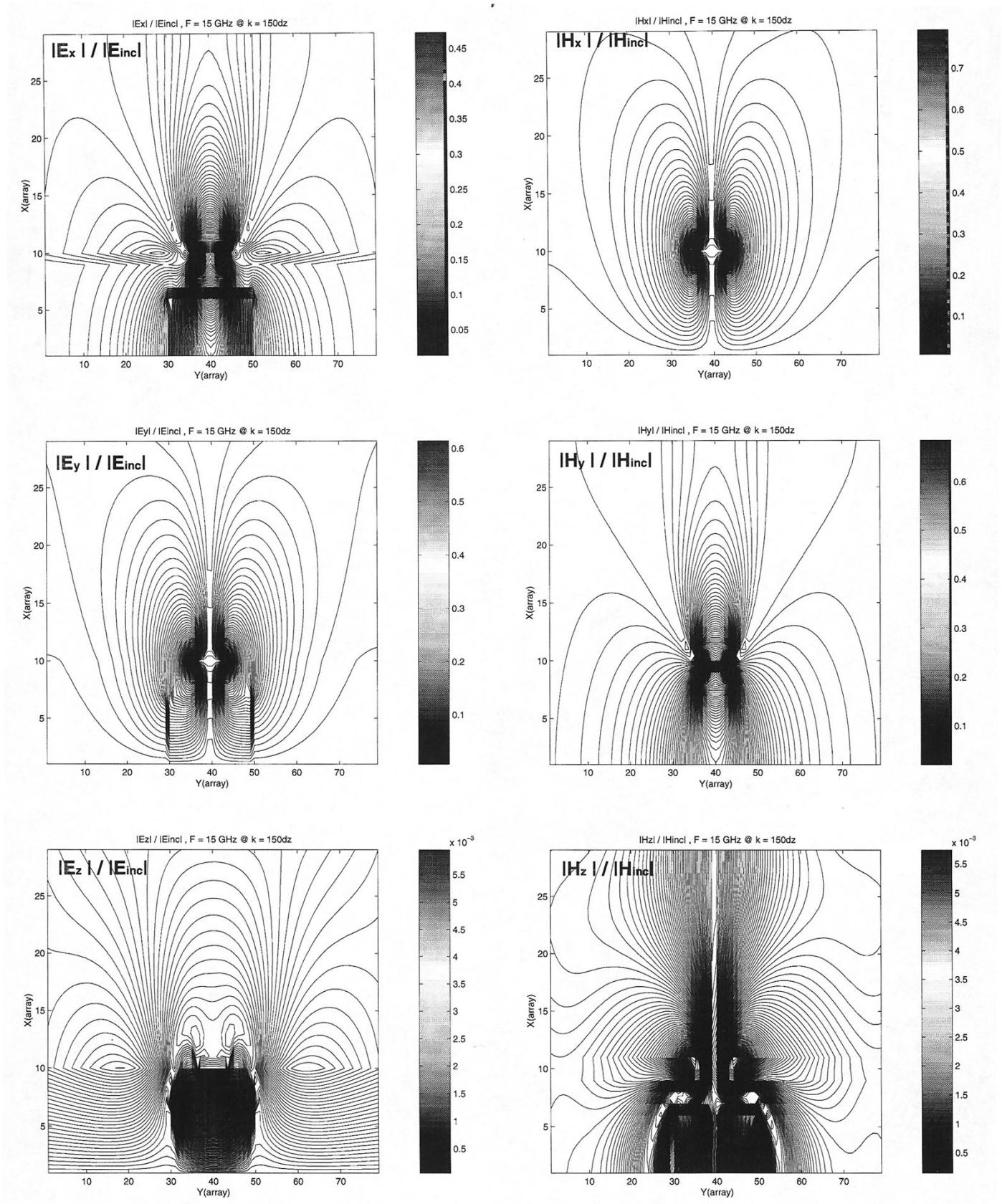

Fig. 3. Normalized electric- and magnetic-field components in the x–y plane at $k = 150dz$, $F = 15$ GHz, $W_1 = 3W_2$.

impedance characteristics are then computed and compared among themselves. Finally, an approximate measure of the conductor and dielectric losses have been presented from the knowledge of the effective dielectric constant, impedance, and current density.

II. Numerical Methods

An extensive analysis and design of the microstrip structures using the FDTD is described in [9], and, hence, is not repeated here. Fig. 1 shows the geometry of the grooved microstrip configuration modeled inside a FDTD lattice of array dimensions nx, ny, and nz. The lattice boundaries are truncated with second-order Liao's absorbing boundary conditions (ABC's) [10] to simulate the free space. However, in the MOL analysis, the ABC is replaced by perfect conducting walls. In calculating the effective dielectric constant of the microstrip line using the FDTD, the propagation constant is first calculated from the Fourier transformation of the field values at two locations along the transmission line. The input impedance is calculated from the knowledge of the voltage difference between the strip and ground plane and the current on the strip. In this case, the strip is terminated with the ABC wall to insure no reflections.

A comprehensive description and detailed formulation involving the MOL is concluded in [11]. Following the analysis procedure with the MOL, the y-dimension is discretized and the propagation is assumed along the z-direction. For the case of a grooved microstrip configuration, as shown in Fig. 1, the permittivity as shown in distribution also varies in one direction, i.e., y, therefore, beside the scalar potentials, the dielectric constant must be also discretized.

III. Results and Discussion

Numerical analysis is carried out for the grooved microstrip configuration on a substrate with $\varepsilon_{R1} = \varepsilon_{R2} = 2.2$ and the dielectric constant of the groove $\varepsilon_g = 1.0$. The dimensions of the enclosures are as $8W_2 \times 10W_2$ for the MOL analysis. For FDTD, a lattice dimension of $nx = 30$, $ny = 40$, and $nz = 300$, spatial steps $dx = dy = dz = 4.2333 \times 10^{-02}$ mm, and a time step $dt = dx/2c$, c being the free-space speed of light are used. In both methods, due to structural symmetry, only half of the structure is modeled. The strip width is assumed to be $W_2 = 0.254$ mm. The height h_1 and h_2 are assumed to be 0.254 and 0.127 mm, respectively.

A. Field Analysis

Fig. 2 shows snapshots of the E_x electric-field component below the strip, at location $k = 150dz$ along the length of the transmission line, for different groove widths W_1 together with the suspended line case. In these snapshots, a dispersion of the Gaussian pulse is observed, as well as faster propagation illustrated in the earlier occurrence of the pulse as the groove width increases. This behavior indicates a decrease in the effective dielectric constant of the structure as the groove width increases, reaching a minimum at the suspended line case. This behavior is observed for the electric field at all other $k = 70, 110$ values and even with large values of $k = 150$ where the Gaussian pulse is more dispersed.

Next, a three-dimensional vertical-cut contour plot of the normalized electric- and magnetic-field components x, y, and z, located on the x–y plane normal to the transmission line at $k = 150dz$ from the excitation plane $(k = 1)$ is presented. The location of the contour plots plane is chosen at $k = 150dz$ to eliminate the presence of evanescent modes and to record only the dominant mode. Fig. 3 shows these contour plots for a groove width $W_1 = 3W_2$ at $F = 15$ GHz. These contours are computed from the time history of the corresponding field components located at the cut-plane by implementing the discrete Fourier transformation (DFT) on each field components. As shown in Fig. 3, high-intensity concentration of the electric-field x, y, and z components are located in the groove region. Not much change is observed for the magnetic-field distribution, suggesting that such a groove geometry has an effect only on the effective permittivity of the grooved microstrip line (GMSL). Such a behavior of the electric and magnetic fields was observed at other frequencies as well (5 and 30 GHz), which suggests that there is no significant change in the dispersive characteristics of the GMSL versus frequency.

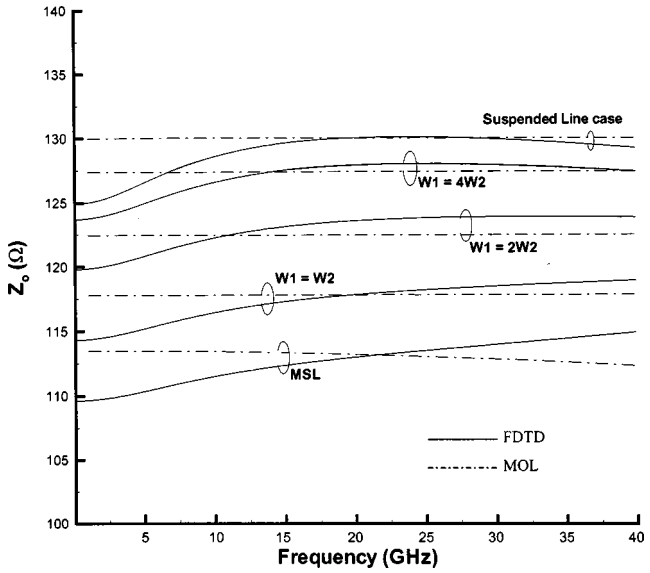

Fig. 4. Characteristic impedance of a GMSL obtained using the FDTD and MOL methods for different groove widths W_1. ($h_1 = 0.127$ mm, $h_2 = W_2 = 0.254$ mm, $\varepsilon_{r1} = \varepsilon_{r2} = 2.2$).

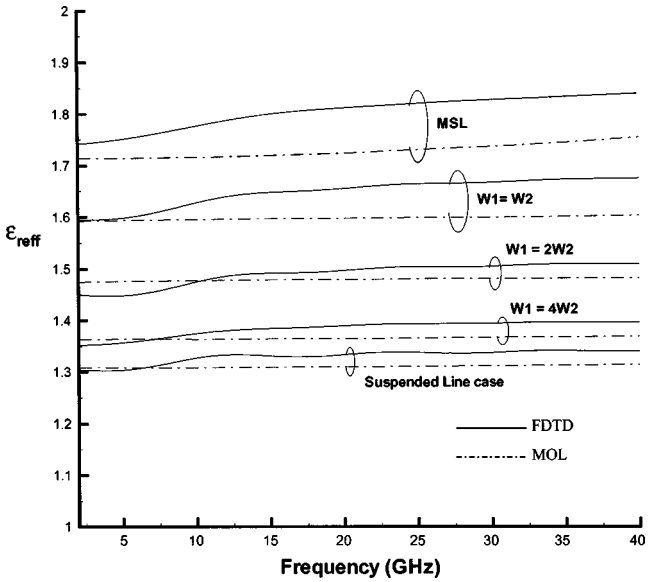

Fig. 5. $\varepsilon_{\mathrm{reff}}$ of a GMSL calculated using the FDTD and MOL methods for different groove widths W_1. ($h_1 = 0.127$ mm, $h_2 = W_2 = 0.254$ mm, $\varepsilon_{r1} = \varepsilon_{r2} = 2.2$).

B. Input Parameters

1) Characteristic Impedance: The input parameters and dispersion characteristics of the GMSL are also calculated using the FDTD and MOL. In the FDTD, input impedance can be calculated from the knowledge of the voltage difference between the strip line and ground plane, the current on the strip in the time domain, and by terminating the strip line by the ABC of the FDTD lattice to eliminate any reflections.

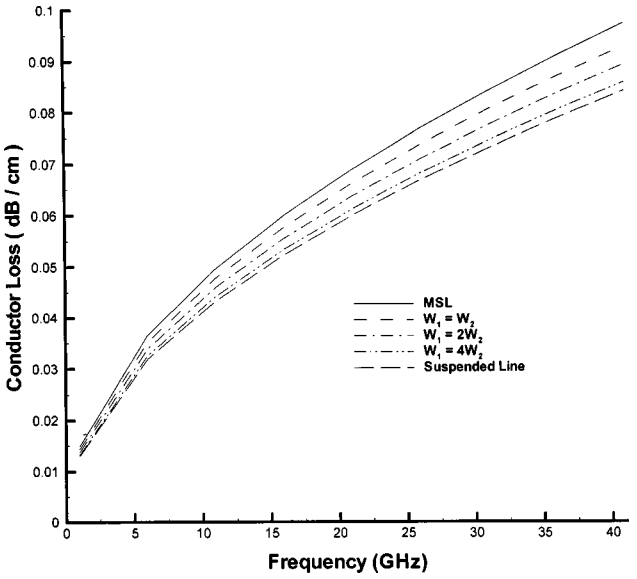

Fig. 6. Conductor loss of a GMSL using the MOL for different groove widths W_1.

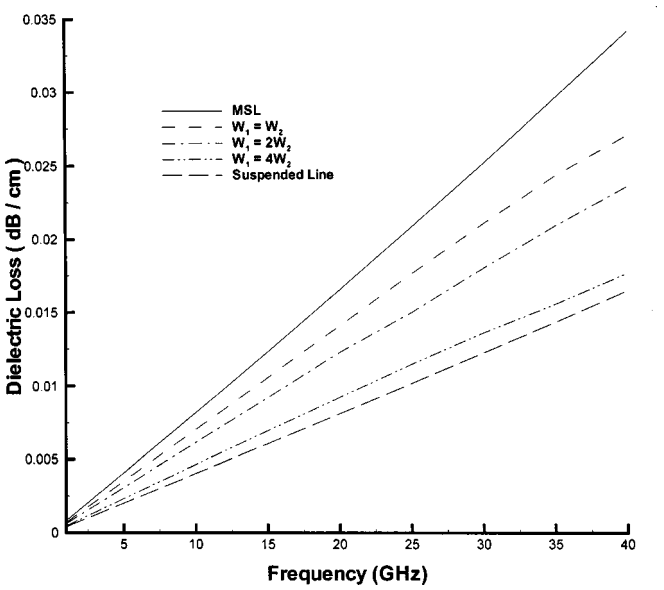

Fig. 7. Dielectric loss a GMSL using the MOL for different groove widths W_1.

Hence, the impedance can be calculated in the frequency domain at location $k = k_{z0}$ along the transmission line as

$$Z_o \left. \frac{V(\omega)}{I(\omega)} \right|_{k=k_{zo}} \tag{1}$$

where $V(\omega)$ and $I(\omega)$ are the frequency-domain voltage and current obtained by the DFT of the time-domain voltage and current. In the case of the MOL, the impedance is obtained from [12] by substituting the value of $\varepsilon_{\text{reff}}$ obtained from MOL calculations. Fig. 4 shows the characteristic impedance of the GMSL obtained from the two methods for different groove widths $W_1 = W_2$, $2W_2$, and $4W_2$, as well as, the simple microstrip (no groove, $W_1 = 0$) and the suspended-line case (very large groove). Both methods agree favorably in showing an increase in the characteristic impedance as the groove width is increased. At low frequencies (<5 GHz), a maximum discrepancy of less than 4% is observed between the two methods for the suspended-line case.

2) Effective Permittivity: In computing the effective dielectric constant of the microstrip line using the FDTD, the complex propagation constant $\gamma(\omega)$ is first calculated from the Fourier transformation of the field values at two locations along the transmission line. The effective permittivity is defined through $\beta(\omega)$, the imaginary part of $\gamma(\omega)$, as

$$\varepsilon_{\text{reff}}(\omega) = \frac{\beta^2(\omega)}{\omega^2 \varepsilon_r \mu_r}. \tag{2}$$

Fig. 5 shows the effective dielectric constant of the GMSL for different groove widths, simple microstrip (no groove), and suspended microstrip-line configurations. The results obtained are then compared with those obtained from the MOL. A good agreement is found between the two methods over the whole frequency band considered. However, it is seen that the effective dielectric constant obtained from the MOL simulation is lower by a maximum of 4.5% than that of the FDTD result. This can be attributed to the fact that the MOL simulation is done for the enclosed configuration, while the in FDTD simulation, the open structure is considered. The effect of the enclosure is seen to diminish with the increase in groove dimension as the less dispersive lines are less affected by the enclosure. The effective dielectric constant of a transmission line mainly depends on the dielectric constant of the material under the strip. Therefore, as the groove dimensions below the strip are increased, the effective dielectric constant of the transmission line decreases, indicating an increase in the volume of the $\varepsilon_r = 1$ space.

3) Conductor and Dielectric Loss: Finally, the conductor and dielectric losses are calculated from the perturbation formula by substituting for the value of impedance and current density [13]. Fig. 6 shows the conductor-loss characteristics as a function of groove width in the frequency range from 1–40 GHz. As seen in the figure, the conductor loss decreases as the groove width is increased. At the same time, partial removal of the dielectric material in the vicinity of the strip conductor reduces the dielectric loss. Fig. 7 shows dielectric-loss characteristics and, as evident from the figure, the dielectric loss also decreases as the groove width is increased. For large groove dimensions, the conductor and dielectric losses are found to be close to those of the suspended line.

IV. Conclusion

The GMSL is studied and analyzed using the FDTD and MOL. A detailed field distribution is presented using the FDTD. The GMSL provides low loss and is found to be less dispersive in comparison to the conventional microstrip lines. It also provides a wide range of impedance values as the groove dimensions add to an extra degree of freedom in varying the impedance.

References

[1] R. S. Tomar and P. Bhartia, "Suspended and inverted microstrip design," *Microwave J.*, pp. 173–178, Mar. 1986.

[2] I. P. Polichronakis and S. S. Kouris, "Computation of the dispersion characteristics of a shielded suspended substrate microstrip line," *IEEE Trans. Microwave Theory Tech.*, vol. 40, pp. 581–584, Mar. 1992.

[3] N. Gupta and L. Shafai, "Grooved suspended microstrip line," in *IEEE Joint AP-S URSI Symp. Dig.*, Atlanta, GA, June 21–26, 1998, pp. 1468–1471.

[4] W. Chamma, N. Gupta, and L. Shafai, "Dispersion characteristics of suspended microstrip line on segment dielectric substrate," in *Antenna Technol. Applied Electromag. Symp. Dig.*, Ottawa, Ont., Canada, Aug. 1998, pp. 159–162.

[5] N. Gupta, N. Jacob, W. Chamma, L. Shafai, S. Raut, and A. Assi, "Simulation and experimental evaluation of the low loss grooved lines," in *Antenna Technol. Applied Electromag. Symp. Dig.*, Ottawa, Ont., Canada, Aug. 1998, pp. 451–454.

[6] V. Milanovic, M. Gaitan, E. D. Bowen, and M. E. Zaghloul, "Micromachined microwave transmission lines in CMOS technology," *IEEE Trans. Microwave Theory Tech.*, vol. 45, pp. 630–635, May 1997.
[7] L. Katehi, G. Rebeiz, T. Weller, R. Drayton, H. Cheng, and J. Whitaker, "Micromachined circuits for millimeter and sub-millimeter-wave application," *IEEE Trans. Antenna Propagat.*, vol. 35, pp. 9–17, Jan. 1993.
[8] N. Dib, W. Harokpus, Jr., P. Katehi, C. Liang, and G. Rebeiz, "Study of a novel planar transmission line," in *IEEE MTT-S Microwave Symp. Dig.*, 1991, pp. 623–626.
[9] X. Zhang and K. Mei, "Timer-domain finite-difference approach to the calculation of the frequency-dependent characteristics of microstrip discontinuities," *IEEE Trans. Microwave Theory Tech.*, vol. 36, pp. 1775–1787, Dec. 1988.
[10] Z. P. Liao, H. Yang, B. Yang, and Y. Yuan, "A transmitting boundary for the transient wave analysis," *Scientia*, vol. 27, no. 10, pp. 1063–1076, Oct. 1984.
[11] R. Pregla and W. Pacsher, "The method of lines," in *Numerical Techniques for Microwave and Millimeter Wave Passive Structures*, T. Itoh, Ed. New York: Wiley, 1989, pp. 381–446.
[12] R. K. Hoffman, *Handbook of Microwave Integrated Circuits*. Norwood, MA: Artech House, 1987.
[13] D. Mirshekar-Syahkal and J. B. Davis, "Accurate solution of microstrip and coplanar structures for dispersion and for dielectric and conductor losses," *IEEE Trans. Microwave Theory Tech.*, vol. MTT-27, pp. 694–699, July 1979.

Microwave Reflection and Transmission Properties of High-Performance Heat Reflective Glass

P. Hui, E. H. Lim, and H. S. Tan

***Abstract*—Microwave reflections from both coated and uncoated sides of high-performance heat-reflective glass (HPHRG) can be minimized by the use of appropriately designed electrically conductive (EC) coatings. Formulas for optimal sheet conductance for the minimization of reflections from HPHRG are presented in this paper. Experimental results are presented for comparison with the theoretical model to confirm these findings.**

***Index Terms*—High-performance heat-reflective glass, microwave reflection/transmission, permittivity.**

I. Introduction

High-performance heat reflective glass (HPHRG) has been widely used for windows and panels in modern building structures. The HPHRG is basically a flat sheet float glass of soda–lime–silicate coated on one side with a thin layer of electrically conductive (EC) film, as shown in Fig. 1(a). Klein [1] has reported results of a study on microwave transmission through EC-coated glass, giving the upper and lower limits of the shielding effectiveness. Niwas *et al.* [2] have studied TV signal reflections from HPHRG in VHF and UHF bands, showing that large sheet resistance of the EC coating in the order of k·Ω/□ is needed to reduce the reflection level from the HPHRG. In [3], we published results that show that the microwave reflection from the uncoated side of HPHRG can be minimized by appropriate choice of the sheet resistance of the EC coating. In this paper, we extend our previous work to study the problem of minimization of microwave reflection from the coated side of the glass sheet.

Manuscript received November 11, 1998. This work was ssupported under the Ministry of Defense/Nanyang Technological University Joint Research and Development Program MINDEF-NTU/09/96.

The authors are with the School of Electrical and Electronic Engineering, Nanyang Technological University, Singapore 639798.

Publisher Item Identifier S 0018-9480(00)02771-X.

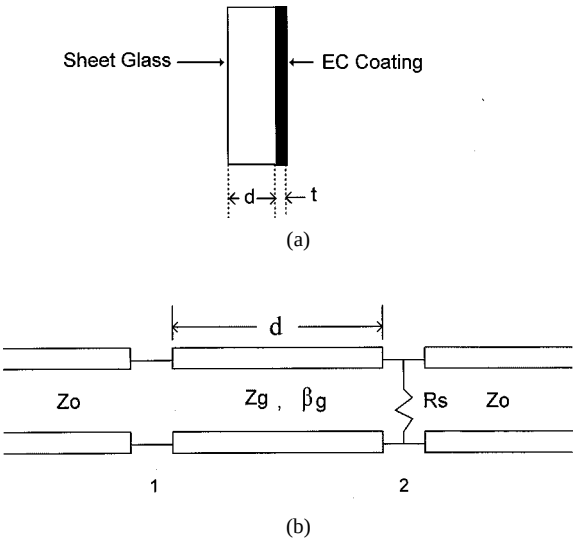

Fig. 1. (a) Structure of HPHRG. (b) Transmission-line model for the HPHRG.

II. Minimaization of Reflections

For an infinite EC coating of thickness t, conductivity σ, permittivity ε, and permeability μ, the good conductor condition $\sigma \gg \omega\varepsilon$ is valid for conductors and semiconductors at microwave frequencies. With t less than a few hundred angstroms, we would have $t \ll \delta$, where $\delta \approx \sqrt{2/\omega\mu\sigma}$ is the skin depth in the order of micrometers. Under these two conditions, we can represent the EC coating as a shunt sheet resistance $R_S \equiv 1/\sigma t$ for both the normal and oblique incidence of electromagnetic waves.

With the transmission-line model shown in Fig. 1(b), we have found [3] that the reflection from the uncoated side of HPHRG can be minimized by the sheet resistance of the EC coating. The normalized sheet conductance for the minimal reflection is given by

$$g_{S\min} = y_g \sqrt{\frac{1 + y_g^2 \tan^2\theta}{y_g^2 + \tan^2\theta}} - 1 \tag{1}$$

where $y_g = Y_g/Y_0$ and $\theta = \beta_g d$ are the phase shift over the glass substrate. There are two special cases worth mentioning. At the half-wavelength resonance $\tan\theta = 0$, we have $g_{S\min} = 0$ and $S_{11} = 0$, meaning that no coating should be used to minimize the reflection level. For the quarter-wavelength configuration $\tan\theta \to \infty$, we obtain $g_{S\min} = y_g^2 - 1$ and $S_{11} = 0$. This condition is equivalent to $Y_g^2/(G_S + Y_0) = Y_0$. In other words, we can adjust the sheet conductance of the EC coating so that the input admittance after the quarter-wave transformer of the sheet glass will be matched to the characteristic admittance of air Y_0, thereby resulting in no reflection from the uncoated side of HPHRG.

After careful examination, we have found that the reflection from the coated side of the HPHRG can also be minimized by the EC coating. The optimized sheet conductance of the EC coating and the minimal reflection coefficient are given as

$$g_{S\min} = \sqrt{b^2 + 1} - g \tag{2}$$

$$|S_{22}|_{\min} = \frac{b}{\sqrt{b^2 + 1} + 1} \tag{3}$$

where

$$b = \frac{y_g\left(y_g^2 - 1\right)\tan\theta}{y_g^2 + \tan^2\theta} \tag{4a}$$

$$g = \frac{y_g\left(1 + \tan^2\theta\right)}{y_g^2 + \tan^2\theta}. \tag{4b}$$

We note that such minimization of reflection from the coated side of HPHRG occurs only when the glass substrate satisfies the following two conditions:

$$\theta < \tan^{-1}\sqrt{\frac{y_g\left(y_g^2 - 3\right)}{y_g^2 + 1}} \tag{5a}$$

$$y_g > \sqrt{3}. \tag{5b}$$

For the half-wavelength resonance, we have $g_{S\,\min} = 0$ and $|S_{22}| = 0$, i.e., no coating should be used. However, for the quarter-wavelength configuration, there is no minimum point for the reflection level from the coated side of HPHRG due to the condition on the phase shift specified by (5a).

III. Measurements

The flat HPHRG samples used are green float glass of soda–lime–silicate of thickness 5.75 mm with titanium–nitride (TiN) EC coatings of thicknesses of 250, 300, and 450 A. Experiments in the R-band (1.7–2.6 GHz) and G-band (3.95–5.85 GHz) have been performed using waveguide sample holders and an HP 8722C vector network analyzer to measure dielectric constants of the glass samples and study the effects of EC coatings on microwave reflection and transmission properties of HPHRG.

A. Uncoated Sheet Glass

We extract the reflection and transmission coefficients directly from the network analyzer, and curve fit the raw data with the transmission-line model [3]. The relative permittivity and loss tangent are determined from the curve fitting. We have checked the accuracy of our measurement and curve-fitting process by using Teflon samples as control measurements. The measured results for Teflon are $\varepsilon_r' = 2.08$ and $\tan\delta = 1.4 \cdot 10^{-4}$, which agreed with published values [4].

For the green float glass, the measured results are $\varepsilon_r' = 6.6$ and $\tan\delta = 0.042$ in the R-band, and $\varepsilon_r' = 6.8$ and $\tan\delta = 0.006$ in the G-band. The detailed results for the green float glass measured in the G-band have been presented in [5]. These values agree well with published values of $\varepsilon_r' = 6.82$ and $\tan\delta = 0.0072$ for soda–lime glass at 10 GHz [6].

For BK7 glass samples of 5.8-mm thickness, the measured dielectric constants are $\varepsilon_r' = 6.2$ and $\tan\delta = 0.002$ in the R-band, and $\varepsilon_r' = 6.3$ and $\tan\delta = 0.0008$ in the G-band. It is noted that BK7 glass is less lossy than the green float glass.

B. Effects of the TiN Coating

We measured the sheet resistance (R_S) of TiN film using a Cascade Microtech C4S-54 four-point probe station. For 5.75-mm HPHRG samples, the measured R_s values are 254 $\Omega/\square$ for the 250 A, 136 $\Omega/\square$ for 300 A, and 83 $\Omega/\square$ for 450 A, corresponding to the calculated electrical conductivity values of $1.57 \cdot 10^5$ S/m, $2.45 \cdot 10^5$ S/m, and $2.67 \cdot 10^5$ S/m, respectively. The difference in conductivity is likely to be due to the variation in actual coating thickness. Nevertheless, we only need values of sheet resistance in our fitting processes for reflection and transmission coefficients. It is noted that the fitted ac sheet resistance is higher than the measured dc sheet resistance, i.e., 275 $\Omega/\square$ for 250 A, 168 $\Omega/\square$ for 350 A, and 100 $\Omega/\square$ for 450 A.

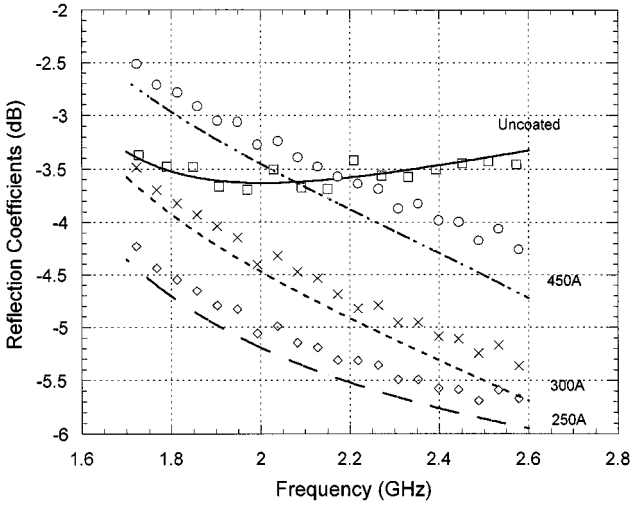

Fig. 2. Measured and fitted reflection coefficient from the uncoated side of 5.75-mm HPHRG with TiN coatings of 250, 300, and 450 in the R-band.

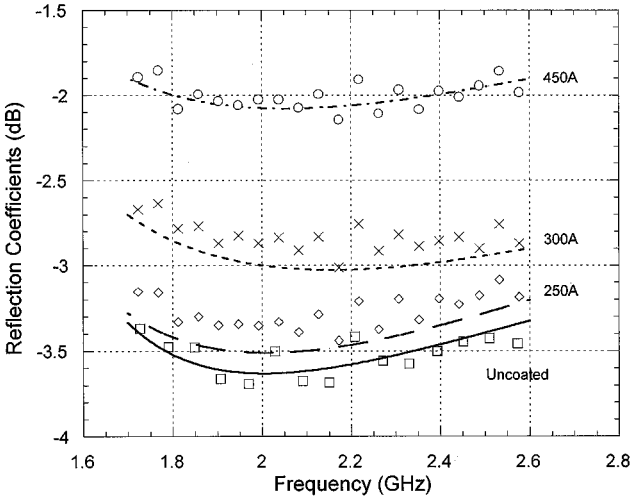

Fig. 3. Measured and fitted reflection coefficient from the coated side of 5.75-mm HPHRG with TiN coatings of 250, 300, and 450 in the R-band.

In Fig. 2, we show the return loss in the R-band from the uncoated side of the three HPHRG samples and one uncoated 5.75-mm soda-lime glass. It is seen that over the frequency range of 1.7–2.6 GHz the return loss has been reduced due to the TiN coatings of 250- and 300-A thickness, as compared to the return loss from the uncoated glass sample. However, for the HPHRG sample with 450-A TiN coating, the return loss increases over the frequency from 1.7 to 2.05 GHz, and decreases over the frequency from 2.05 to 2.8 GHz compared with that of uncoated glass. The experimental and fitted results clearly indicate that the reflection coefficient from the uncoated side of HPHRG can be reduced by the presence of the EC coating, and there exists an optimal EC-coating thickness (or sheet resistance) for the minimization of reflection.

The reflection coefficients from the coated side of the HPHRG samples and the uncoated glass sample in the R-band are shown in Fig. 3. First, we observe that, for each coating thickness, the reflection from

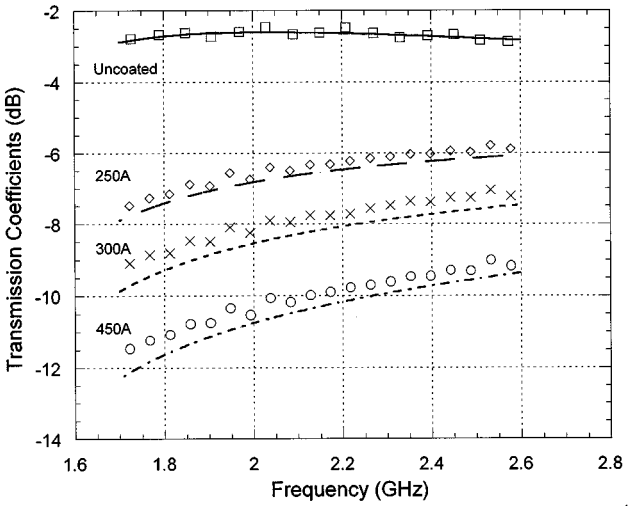

Fig. 4. Measured and fitted transmission coefficient through 5.75-mm HPHRG with TiN coatings of 250, 300, and 450 in the R-band.

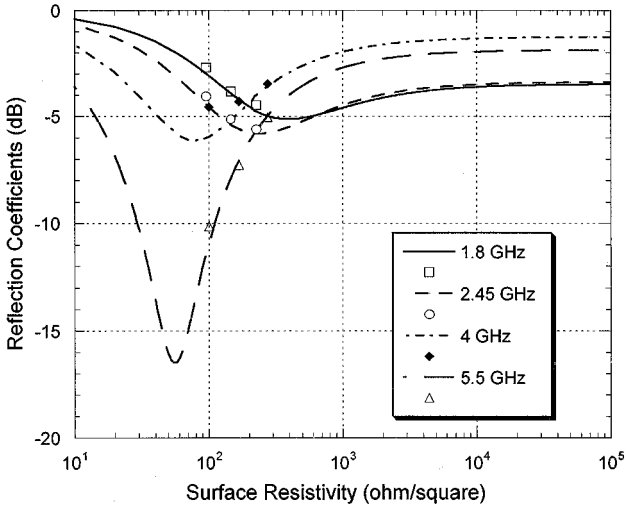

Fig. 5. Reflection from the uncoated side of 5.75-mm HPHRG with $\varepsilon_r = 6.8$ and $\tan\delta = 0.0106$ with respect to the sheet resistance.

the coated side of HPHRG samples is always higher than from the uncoated side. Second, as the coating thickness increases (equivalent to reducing the sheet resistance), the reflection level increases. We do not find any minimum of reflection level for the three HPHRG samples. As calculated using (2), the optimal R_S for a 1.8-GHz frequency is about 600 $\Omega/\square$. For the three HPHRG samples used, the sheet resistances are from 83 to 254 $\Omega/\square$, which is too low to produce a reflection minimum from the coated side of HPHRG in the R-band.

The transmission coefficients in the R-band are shown in Fig. 4. It is seen that the transmission through HPHRG has been reduced from 4 to 3 dB for a 250-A coating, from 7 to 4 dB for a 300-A coating, and from 9 dB to 6 dB for a 450-A coating as compared to those of uncoated glass.

C. Minimization of Reflection Coefficients

To further verify the phenomena of minimization of reflection due to the sheet resistance of the EC coating, we plot in Fig. 5 the theoretical and experimental return loss from the uncoated side of the 5.75-mm HPHRG sample as a function of R_S at four different frequencies of 1.8, 2.45, 4, and 5.5 GHz. As R_S increases from 83 to 254 $\Omega/\square$, the return loss is reduced for frequencies of 1.8 and 2.45 GHz, but increased for 4 and 5.5 GHz. It is clear that the EC coating can be used to minimize the microwave reflections from the uncoated surface of HPHRG. The reduction of the level of the return loss at the minimum point as compared to that of the uncoated glass depends on the phase shift through the sheet glass. For the special case of quarter-wavelength configuration $\theta = 90^\circ$, the reduction reaches the maximum, being null reflection if glass is lossless. Ignoring the small loss tangent and using $\varepsilon_r = 6.8$, we have calculated the guided wavelength of the sheet glass to be 6.68 cm for 1.8 GHz, 4.81 cm for 2.45 GHz, 3.02 cm for 4 GHz, and 2.14 cm for 5.5 GHz. The corresponding phase shifts through the 5.75-mm sheet glass are 31.0°, 43.1°, 68.6°, and 96.5°, respectively. It is seen in Fig. 5 that as frequency increases, the phase shift becomes larger and approaches 90°, thereby causing a larger reduction in the return loss at the minimum point.

Similar results for the reflection coefficients from the coated side of the HPHRG samples with respect to the sheet resistance are shown in Fig. 6. As the sheet resistance reduces from 254 to 83 $\Omega/\square$, corresponding to the coating thickness increasing from 250 to 450 A, the

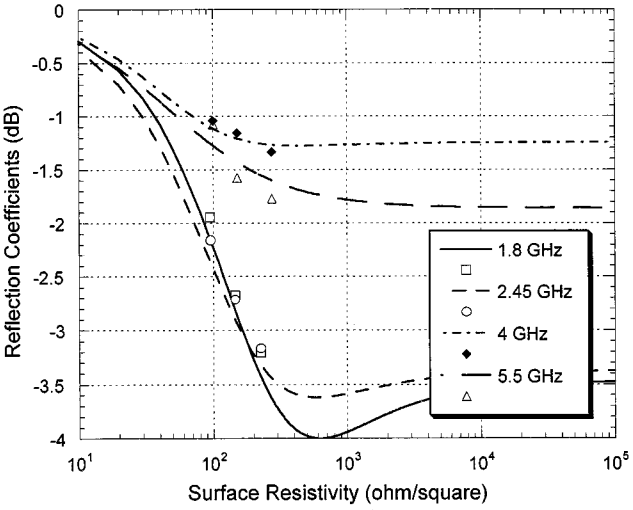

Fig. 6. Reflection from the coated side of 5.75-mm HPHRG with $\varepsilon_r = 6.8$ and $\tan\delta = 0.0106$ with respect to the sheet resistance.

reflection from the coated side of HPHRG increases for all four frequencies. The theoretical calculations using (2) indicate that there are minimum points for frequencies of 1.8, 2.45, and 4 GHz, as shown in Fig. 6. However, the reduction at these minimal reflection points as compared to the reflection levels for the uncoated sheet glass is smaller than 0.5 dB.

IV. Conclusion

In addition to the minimization of the reflection from the uncoated side of HPHRG, our results show that the reflection level from the coated side of HPHRG can also be minimized by the EC coating, but only for certain phase-shift range of the sheet glass. At the minimum point, the reduction of the reflection level from the coated side of the HPHRG is not as significant as the reduction of reflection from the uncoated side. Formulas for the optimized sheet resistance for minimizing the reflection from both uncoated and coated sides of the HPHRG have been given. Experimental results have been compared with the results of our transmission-line model to confirm the findings.

ACKNOWLEDGMENT

The authors would like to thank A/Prof. P. Hing, School of Applied Science, Nanyang Technical University, Singapore, for making available the use of the measurement equipment in his laboratory. The authors are also grateful to C. Ng, Asahi Allglass (Asia) Pte Ltd., Singapore, for his assistance in providing HPHRG samples, and to K. Chin Bong, Avimo Electro-Optics Pte Ltd., Singapore, for his assistance in the sample preparation.

REFERENCES

[1] C. A. Klein, "Microwave shielding effectiveness of EC-coated dielectric slabs," *IEEE Trans. Microwave Theory Tech.*, vol. 38, pp. 321–324, Mar. 1990.
[2] H. Niwa, H. Ito, Y. Hashimoto, H. Kurihara, and K. Ishino, "Investigation on TV wave reflecting characteristics of high performance heat-reflective glass and its improvement," in *Proc. IEEE Int. Electromag. Compat. Symp.*, Miyai, Japan, 1994, pp. 359–362.
[3] P. Hui, E. H. Lim, and H. S. Tan, "Minimization of microwave reflections from EC-coated glass slabs," *IEEE Microwave Guided Wave Lett.*, vol. 8, pp. 363–365, Nov. 1998.
[4] A. R. Von Hipple, *Dielectric Materials and Applications.* New York: Wiley, 1954.
[5] P. Hui, E. H. Lim, and H. S. Tan, "Microwave reflection and transmission of high performance heat reflective glass in the frequency range from 3.95 to 5.85 GHz," in *Proc. 4th Asia–Pacific Commun. Conf./6th Singapore Int. Commun. Syst. Conf.*, Singapore, Nov. 23–27, 1998, pp. 874–878.
[6] E. J. Vanzura, J. R. Baker-Jarvis, H. H. Grosvenor, and M. D. Janezic, "Intercomparison of permittivity measurements using the transmission/reflection method in 7-mm coaxial transmission lines," *IEEE Trans. Microwave Theory Tech.*, vol. 42, pp. 2063–2070, Nov. 1994.

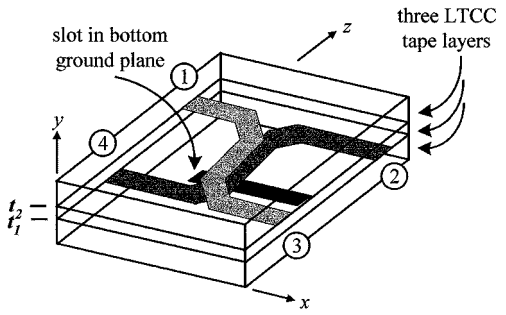

Fig. 1. Broadside coupler buried in LTCC (port numbers circled). Additional LTCC layers (not shown) cover the top ground plane.

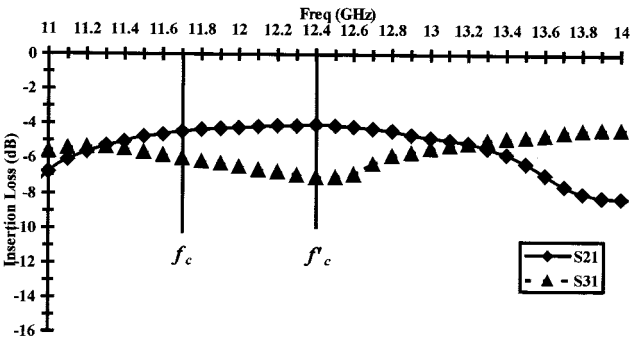

Fig. 2. Insertion loss of broadside coupler with uniform ground planes on top and bottom of LTCC. Center frequency at 12.4 GHz.

Tunable Microwave Coupler Buried in Low-Temperature Co-Fired Ceramic

Scott A. Wartenberg

***Abstract*—This paper outlines a method of tuning a microwave broadside coupler buried in low-temperature co-fired ceramic. Etching a slot in the exposed ground plane tunes the characteristic impedance Z_0 of a stripline coupler. An iterative method computes the correct dimensions of the slot. Applying the method salvages microwave circuits detuned due to manufacturing tolerances.**

***Index Terms*—Co-fired, low temperature, multilayer ceramic, stripline coupler.**

I. INTRODUCTION

During firing of multilayer ceramics, the thickness t of each layer has a tendency to grow or shrink about $+/-10\%$, resulting thickness $t' = t+/-0.10t$. The conductive paste used for the buried conductors (width w) also has growth or shrinkage on the same order (resulting stripline width $w' = w+/-0.10w$). Changes in the ceramic thickness and conductor width impact the microwave impedance of the lines. Since they are inaccessible, the conductors cannot be trimmed. An inexpensive solution is to etch a slot in the ground plane exposed on the bottom side of the low-temperature co-fired ceramic (LTCC). This technique retunes the coupler by changing the even-mode impedance $Z_{\rm even}$ and, to a lesser degree, the odd-mode impedance $Z_{\rm odd}$. During LTCC processing, the bottom ground-plane metallization is omitted. Afterwards, the dimensions are measured and a slotted ground plane is thin-film deposited on the bottom of the post-fired board (Fig. 1).

II. THEORY

An iterative approach determines electromagnetic perturbation effects by the slot on a broadside coupler. The approach consists of the following five steps [1].

Step 1: For a broadside coupler with uniform ground planes (i.e, no slot), find the electric surface current $\mathbf{J}$ for the even and odd modes of each conductor using conventional TEM-wave analysis [2], [3].

Step 2: Separate the problem into two physical regions [4], [5]. For a slotted ground plane at $y = 0$, the conductors are in the $y > 0$ region. The tangential electric field $\mathbf{E_t}$ of the slot is replaced by an equivalent magnetic surface current $\mathbf{M}$. In the $y < 0$ region, $-\mathbf{M}$ likewise replaces $\mathbf{E_t}$. Expressions in the spectral domain are written for the magnetic fields $\mathbf{H}\sim$ in the two regions. Continuity of the tangential magnetic field $\mathbf{H_t}\sim$ for the slot at $y = 0$ relates the two regions $y < 0$ and $y > 0$. Applying the spectral-domain immitance approach gives the spectral Green's functions $\mathbf{G}\sim$ and the unknown $\mathbf{M}\sim$ [6].

Step 3: Knowing $\mathbf{G}\sim$, $\mathbf{M}\sim$ from Step 2 and $\mathbf{J}\sim$ from Step 1, calculate the transverse electric field $\mathbf{E_t}\sim$ on the striplines at $y = t_1, t_2$.

Manuscript received January 14, 1999.
The author is with Agilent Technologies, Newark, CA 94560 USA (e-mail: scott_wartenberg@agilent.com).
Publisher Item Identifier S 0018-9480(00)02777-0.

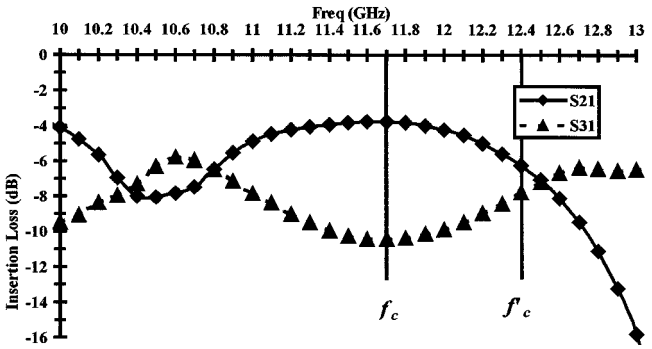

Fig. 3. Insertion loss of broadside coupler with slotted ground plane on bottom. Center frequency shifts to 11.7 GHz.

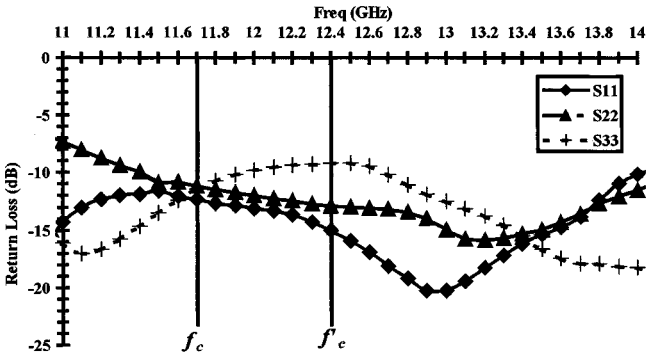

Fig. 4. Return loss for unterminated ports of LTCC broadside coupler with uniform ground planes.

Step 4: Using $\mathbf{E_t} \sim$, find $\mathbf{J}$ and proceed again to Step 2. Iterate until the solution converges.

Step 5: Using the even- and odd-mode converged solutions, calculate Z_0 or the S-parameters.

A computer program expedites the procedure by entering specific slot dimensions and simulating the S-parameters.

III. Experiment

Fig. 2–5 show the performance of an LTCC broadside coupler with uniform ground planes above and below. Using standard LTCC design rules, the intended center frequency f_c was 11.75 GHz with a 3-dB bandwidth $\mathrm{BW}_{3\,\mathrm{dB}}$ of 2.0 GHz. After fabrication, f_c' measured 12.4 GHz with $\mathrm{BW}_{3\,\mathrm{dB}}$ of 2.8 GHz. X-ray analysis revealed the post-fired LTCC board dimensions t' and w'. A slot was then computed and thin-film deposited on the bottom of a coupler cut from the same LTCC. The new f_c measured 11.70 GHz with a $\mathrm{BW}_{3\,\mathrm{dB}}$ of 2.2 GHz. Refinement of the technique should allow narrower coupling bandwidth and less loss.

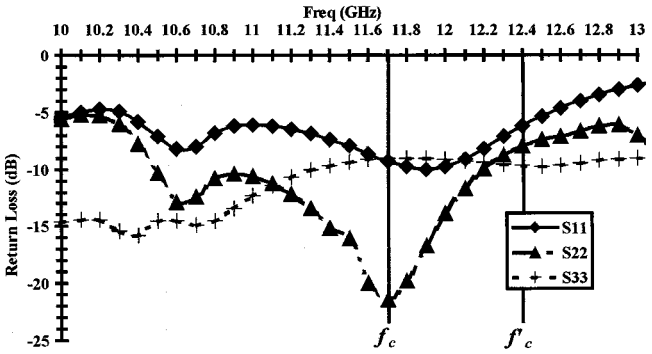

Fig. 5. Return loss for unterminated ports of broadside coupler with slot in exposed ground plane on bottom of LTCC board.

IV. Summary

Using this technique can significantly enhance the yield of LTCC boards containing microwave circuits detuned from ceramic shrinkage or conductor paste squeeze out.

Acknowledgment

The author thanks R. Joseph, The Johns Hopkins University, Baltimore, MD, J. McNulty, The Johns Hopkins University, Baltimore, MD, and C. R. Westgate, The Johns Hopkins University, Baltimore, MD, A. Kouki, L'Ecole Polytechnique de Montreal, Montreal, P.Q., Canada, and G. Lee, Hewlett-Packard Laboratories, Palo Alto, CA, for their helpful suggestions.

References

[1] A. Kouki, R. Mittra, and C. H. Chan, "Analysis of a thin slot discontinuity in the reference plane of a microstrip structure," *IEEE Trans. Microwave Theory Tech.*, vol. 41, pp. 1356–1362, Aug. 1993.

[2] M. K. Krage and G. I. Haddad, "The characteristic impedance and coupling coefficient of coupled rectangular strips in a waveguide," *IEEE Trans. Microwave Theory Tech.*, vol. MTT-16, pp. 302–307, May 1968.

[3] R. R. Gupta, "Accurate impedance determination of coupled TEM conductors," *IEEE Trans. Microwave Theory Tech.*, vol. MTT-17, pp. 479–489, Aug. 1969.

[4] C. H. Chan, K. Ng, and A. Kouki, "A mixed spectral-domain approach for dispersion analysis of suspended planar transmission lines with pedestals," *IEEE Trans. Microwave Theory Tech.*, vol. 37, pp. 1716–1723, Nov. 1989.

[5] A. Kouki, C. H. Chan, and R. Mittra, "A spectral domain approach to electromagnetic coupling through apertures in planar conducting surfaces," *Microwave Opt. Technol. Lett.*, vol. 2, no. 3, pp. 85–88, Mar. 1989.

[6] T. Itoh, "Spectral domain immitance approach for dispersion characteristics of generalized printed transmission lines," *IEEE Trans. Microwave Theory Tech.*, vol. MTT-28, no. 7, pp. 733–736, 1980.